Journal of Metals, Materials and Minerals, 36(2), e2369, 2026

Sintering behavior and mechanical properties of HA-YSZ-Ti Composite sintered by spark plasma sintering

Seyed Mohsen FATEMI[1], Iman MOBASHERPOUR[1,*], Leila NIKZAD[1], and Mansour RAZAVI[1]

[1] *Department of Ceramics, Materials and Energy Research Center (MERC), Karaj, Alborz, Iran*

***Corresponding author e-mail**: I.Mobasherpour@merc.ac.ir

Received date:
6 April 2025
Revised date:
25 September 2025
Accepted date:
19 February 2026

Keywords:
Hydroxyapatite
Composite;
Spark Plasma Sintering;
Mechanical properties

Abstract

This research is aimed to determine the best composition of composite fabricated by Spark Plasma Sintering (SPS) to produce a suitable substituent for bone. The applied powder was prepared by the SPS method and comprises hydroxyapatite (HA), yttria-stabilized zirconia (YSZ), and titanium (Ti). Different percentages of components were used to fabricate the composite samples. X-ray diffraction was used to determine the structural phase of the sintered samples while field emission scanning electron microscopy (FE-SEM) was employed for microstructural analysis of the specimens. The behavior of the samples was investigated during sintering. The gas release, displacements, and porosity percentage of the composite samples were also explored. Three-point bending test was utilized to determine the flexural strength whereas the hardness of the samples was determined by the Vickers method. Moreover, the CHANTIKUL method was used to evaluate the toughness of the samples. The results showed the best mechanical properties in the 90%HA-6%YSZ-4 %Ti sample.

1. Introduction

Humans may experience various damages to their bone throughout their life. Accidents, bone fractures, and joint replacements require bone replacement, further highlighting the importance of a suitable material for bone replacement. In addition to similarity to bone, the mentioned composition should be highly biocompatible and non-toxic. Hydroxyapatite [$Ca_{10}((PO)_4)_6(OH)_2$] with the calcium-to-phosphorus ratio of 1.67 is chemically similar to bone, resulting in its wide application in orthopedic treatments, cosmetic surgeries, and dentistry. About 70% of bone weight is made up of hydroxyapatite. Cells do not differentiate between hydroxyapatite and bone due to their similar surface chemistry, allowing hydroxyapatite to grow on itself, such as osteoblasts. These properties, as well as its high biocompatibility and non-toxicity, make this material a suitable substituent for bone [1–5]. The main drawback of hydroxyapatite is its weak mechanical properties, which could be improved by reinforcement with ceramic or metal powders [6]. Zirconia oxide (ZrO_2) is a chemically stable ceramic material with negligible cellular and tissue affinity and little toxicity. This material enjoys high toughness, mechanical strength, and modulus of elasticity [7]. The introduction of yttrium oxide (Y_2O_3) to the structure of zirconium oxide (ZrO_2) promotes the stability of the cubic crystal structure of ZrO_2 at room temperature. This material has high strength and toughness [8].

Titanium metal has found extensive application orthopedics due to its low density and excellent corrosion resistance. The incorporation of titanium to hydroxyapatite improves the physical properties and biocompatibility of Ti-HA composite [9].

During hydroxyapatite sintering, hydroxyapatite decomposes by raising the sintering temperature, producing oxy apatite, alpha tricalcium phosphate, beta tricalcium phosphate, and tetra calcium phosphate which declines the mechanical properties of the sintered composites [10,11].

The spark plasma sintering (SPS) is a new and highly efficient sintering technique that offers many advantages over traditional sintering methods. These advantages include high speed, lower sintering temperatures, preservation of microstructure and phase composition, high density, and relative simplicity. Since the sintering time in SPS is very short (usually a few minutes), the materials are less exposed to high temperatures. Also, due to the simultaneous application of pressure and electrical pulses (which create plasma and localized heat), the temperatures required for sintering are lower than in traditional methods [12]. These two advantages (high speed and lower temperature) are crucial for a composite such as HA-YSZ-Ti because hydroxyapatite is prone to decomposition into other phases (such as tricalcium phosphate) at high temperatures, and SPS helps maintain the stability of HA by reducing time and temperature. In addition, SPS helps maintain the nanoscale or fine-grained microstructure, which in turn leads to improved mechanical properties. It also prevents unwanted reactions between HA, YSZ, and Ti at high temperatures. Another advantage of SPS is that near-theoretical densities can usually be achieved, which is very important for achieving excellent mechanical properties of the composite. The process is also relatively simple and samples with different shapes can be produced [13,14].

Our goal of creating the ternary composite (HA-YSZ-Ti) is to create that has the strength and durability of titanium, the toughness and fracture resistance of YSZ, and the bioactivity of HA for faster and better bone bonding. This could lead to a durable and efficient implant that is well accepted by the human body. This research is to improve the mechanical properties of hydroxyapatite by incorporation of YSZ

and titanium using the SPS method. The best combination for this method was also determined.

2. Materials and method

2.1 Materials

The components used in this work were commercially available powders. The hydroxyapatite powder in micron sizes was supplied from Merck. Also, commercial powders of zirconia stabilized with yttria (YSZ: ZrO_2 - 3 mol% Y_2O_3) and titanium in micron sizes were used.

2.2. Preparation of composite samples

Different powders with different contents were used at different maximum outer surface of graphite crucible temperature to make composite samples, as listed in Table 1. According to research [15,16], it was found that adding titanium to the hydroxyapatite composition leads to increased thermal decomposition, and if the titanium content reaches above 5%, the sintered samples will crumble and break due to increased thermal decomposition. Therefore, the amount of titanium was chosen to be constant at 4% so that, while benefiting from the properties of titanium in sintered composite samples, thermal decomposition would occur less frequently, and in the ternary composite composition, with constant titanium, it would be possible to examine the effect different percentages of hydroxyapatite and YSZ.

To make composite samples, first, the samples were weighed according to Table 1 with an accuracy of 0.0001 gr. Then, a ball mill was used for 4 h to achieve a uniform mixture.

2.3 Fabrication of composite samples

Spark plasma sintering method was used to prepare composite samples. In a typical procedure, 10 gr of the powder mixture (as mentioned in Table 1) was transferred to a mold (made of graphite with diameter of 30 mm) and pressed by a mandrel. Graphite foil was used to prevent stocking of powders to the mold. After placing the mold and connecting the thermocouple, the door of the vacuum chamber was closed and the vacuum pump system was turned on. The current was applied after reaching vacuum (pressure below 50 Pa). The initial pressure was 10 MPa. The sample started to heat up by applying electric current. Pressure was applied during the sintering process, raising the pressure to 30 MPa. The sample was maintained at the maximum temperature for 5 min, followed by cooling down at different rates. The thickness of the samples produced after the sintering process was about 5 mm.

2.4 Characterizations of HA-YSZ-Ti composites

The size of the powders was measured by the particle size analysis (PSA) in terms of the average size and size distribution.

X-ray diffraction (XRD) method was used to explore the structural phases of the composite. Cu (Kα) beam was used as X-ray source. The residence time in each step, step size, and scanning range were 1 s, 0.02°, and 20° to 70°. For phase analysis of the samples, X-ray diffraction pattern should be matched with the JCPDS patterns using X-ray software.

The microstructure of the samples was explored by a high-resolution scanning electron microscope (SEM) at a voltage of 20 kV. Sample preparation involved sputter deposition of gold on the surface of the samples.

For the three-point flexural strength evaluations, samples were cut by a diamond blade into dimensions of 20 mm × 5 mm × 3 mm followed by surface polishing. The test was performed according to the ASTM C1161-13 standard using a Santam device. This device can apply loads of up to 2 tons. Through the software, it can also record and plot force against displacement. The pressure was applied at the rate of 0.5 mm·min^{-1}. The equation 1 was used to determine the flexural strength of sintered composite samples.

$$\sigma = \frac{3PL}{2bd^2} \quad (1)$$

Where σ is the 3-point (flexural) strength in megapascals, F shows the breaking force in newtons, L, w, and h are respectively the distance of the machine supports, width, and height of the samples in millimetres.

Vickers hardness tester was employed to measure the hardness of the samples according to the ASTM C13227-08 standard. The hardness of the samples was evaluated under a 100 g load with a holding time of 10 s. The test was repeated at least 5 times to obtain an average hardness value. the Chantikul method was used to determine the toughness of the samples [17].

Table 1. Chemical composition and maximum outer surface of graphite crucible temperature of prepared samples.

No	sample code	Composition [wt%]	Maximum outer surface of graphite crucible temperature [°C]
1	100-0-0	100% HA	750
2	90-6-4	90% HA - 6% YSZ - 4% Ti	800
3	81-15-4	81% HA - 15% YSZ - 4% Ti	860
4	75-21-4	75% HA - 21% YSZ - 4% Ti	770
5	70-26-4	70% HA - 26% YSZ - 4% Ti	860
6	65-31-4	65% HA - 31% YSZ - 4% Ti	880

Table 2. D50 values of HA, YSZ and Ti powders.

D50 [μm]	HA	YSZ	Ti
	3.87	36.77	53.81

3. Results and discussion

3.1 Particle size analysis

Figure 1 presents the results of particle size analysis of hydroxyapatite, titanium, and YSZ powders. Also, the minimum diameter equivalent to 50% of the particles of the powders was used to make composite samples as listed in Table 2. The results indicated the proper and uniform size distribution of hydroxyapatite particles with average size of 3.87 µm. The average size of the YSZ and titanium powders was about 36.77 µm and 53.81 µm, respectively. Titanium powders are larger than YSZ, while its size range distribution was close to that of YSZ. The use of a fine matrix powder with coarse reinforcement is a deliberate processing strategy to maximize packing density, ensure a continuous matrix, and facilitate sintering. Moving to a similar particle size distribution would introduce porosity and microstructural heterogeneity, causing a general degradation of all key mechanical properties.

3.2 XRD patterns

The X-ray diffraction results of sintered composite, as well as pure hydroxyapatite, pure titanium and YSZ powders, are shown in Figure 2. The pure hydroxyapatite powder showed a short and broad peak, suggesting its low crystallinity. The 100-0-0 sample exhibited sharp peaks with a small width, reflecting its high crystallinity. The results of composite samples sintered with hydroxyapatite powder revealed the TCP phase, suggesting partial decomposition of hydroxyapatite during the sintering process. According to Figure 2, it can be seen that by decreasing the amount of hydroxyapatite from sample 4 to 9, the intensity of the hydroxyapatite peak in the X-ray diffraction pattern has decreased. On the other hand, by increasing YSXZ, the intensity of this phase in the X-ray diffraction pattern has increased. The presence of the tricalcium phosphate phase due to the decomposition of hydroxyapatite is evident in the X-ray diffraction pattern. In the composite samples, it seems that due to the presence of YSZ and Ti phases, the intensity of the X-ray diffraction pattern of the tricalcium phosphate phase is higher than that of the sample without the reinforcing phase.

All sintered composites exhibited thermal decomposition and the formation of tricalcium phosphate (TCP) through the following reaction 2 [16,18].

$$Ca_{10}(PO_4)_6(OH)_2 \rightarrow 3Ca_3(PO_4)_2 + CaO + H_2O \quad (2)$$

Moreover, the presence of titanium in the composition of composite samples can be effective in the following reaction (3-4) [16,18].

$$Ti + 2H_2O\,(g) \rightarrow TiO_2 + 2H_2\,(g) \quad (3)$$

$$Ca_{10}(PO_4)_6(OH)_2 + TiO_2 \rightarrow 3Ca_3(PO_4)_2 + CaTiO_3 + H_2(g) + \tfrac{1}{2}O_2(g) \quad (4)$$

The formation of both TiO_2 and $CaTiO_3$ are secondary reactions that occur due to the presence of titanium (Ti) in the composite during sintering. For TiO_2, this is an oxidation reaction where metallic titanium (Ti) reacts with water vapor ($H_2O(g)$) present in the sintering atmosphere. For $CaTiO_3$, this is a more complex reaction where the newly formed TiO_2 interacts with the hydroxyapatite ($Ca_{10}(PO_4)_6(OH)_2$) matrix. The reaction consumes both TiO_2 and hydroxyapatite, producing tricalcium phosphate ($Ca_3(PO_4)_2$), calcium titanate ($CaTiO_3$), and gases according reaction 3 and 4. the presence of titanium leads to reactive sintering, forming TiO_2 and $CaTiO_3$. While these phases enhance hardness, wear resistance, and most importantly, interfacial strength, they do so at the cost of reducing the metallic titanium content and altering the original composition. The outgassing from reactions 3 and 4 can also affect the final sintering quality and cause increased porosity. Increased porosity causes a decrease in the mechanical properties of the final composite sample.

Since partial yttria-stabilized zirconia has little reactivity with calcium oxide, it causes less decomposition of hydroxyapatite. On the other hand, the titanium and TiO_2 together with CaO, like yttria, can partially enter the structure of zirconia and cause its full saturation and stability, further promoting stability in YSZ in sample 65-31-4. In the case of 70-26-4 and 65-31-4, the YSZ peak slightly shifted to the right, confirming the entry of calcium oxide into the YSZ structure, as also reported by Heimann and Vu [19,20].

This phenomenon declined the decomposition of hydroxyapatite, which emerged as a decrease in the intensity of the TCP peak in the sample 65-31-4. Moreover, in the sintered composites, a decrement in the HA content and a rise in the YSZ level enhanced the intensity of the peak related to tetragonal zirconia. The titanium phase was not observed in the sintered composite samples, due to its low amount.

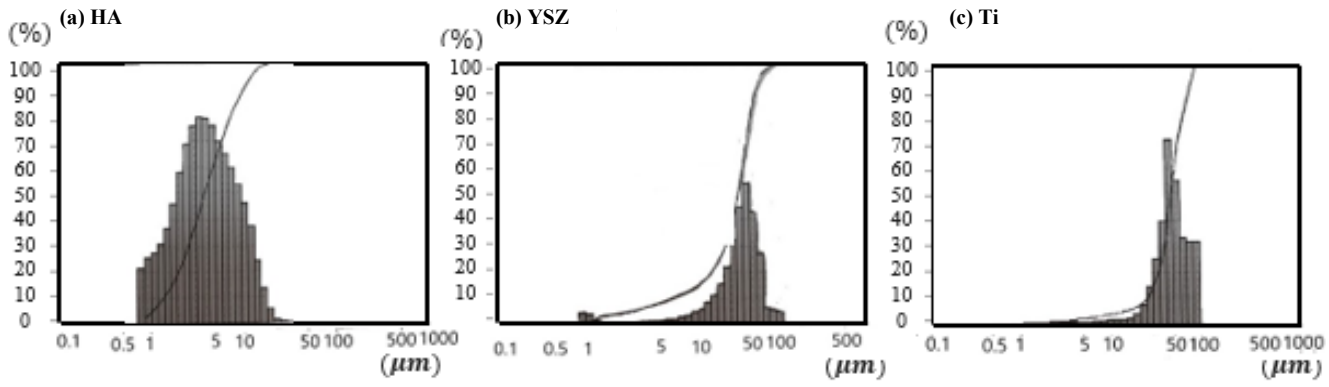

Figure 1. particle size analysis of (a) HA, (b) YSZ, and (c) Ti powders.

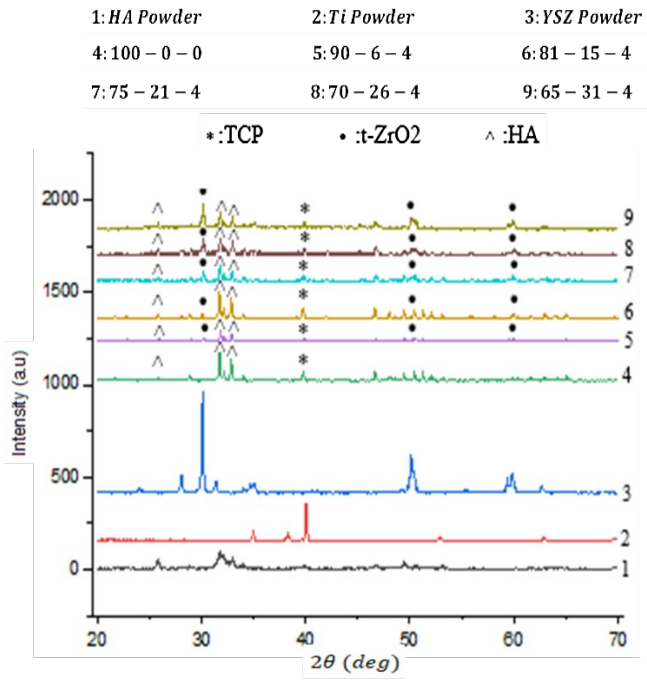

Figure 2. X-ray diffraction test results of sintered samples along with used powders.

3.3 Field emission scanning electron microscope

The results of field emission scanning electron microscopy of the fracture surface of sintered composite samples are shown in Figure 3. As can be seen, the 100-0-0 showed a brittle fracture. The images of other sintered composites exhibited softer fracture cross-section. Regarding the D50 of the YSZ powder (~ 37 µm), the circular shapes in the images of the sintered composite samples are related to the YSZ powder; it was found that the used YSZ powder was mostly spherical.

In the sintered composite samples, a rise in the percentage of YSZ up to 26% enhanced these circular shapes. These particles are located in the grain boundaries where the failure occurred. Porous parts can be seen in some of the sintered composites. These parts are related to the decomposition of hydroxyapatite and the presence of TCP phase. Noteworthy, the fracture surface contained these areas.

During the sintering process of the composite samples, YSZ powders did not reach the sintering stage.

In some parts where the YSZ powder particles are placed next to each other, sintering did not occur between the YSZ particles, forming places that are not bonded to the ground, hence decreasing the mechanical properties. The YSZ powders are better mixed with the hydroxyapatite powders in sample 65-31-4, explaining its higher maximum sintering temperature.

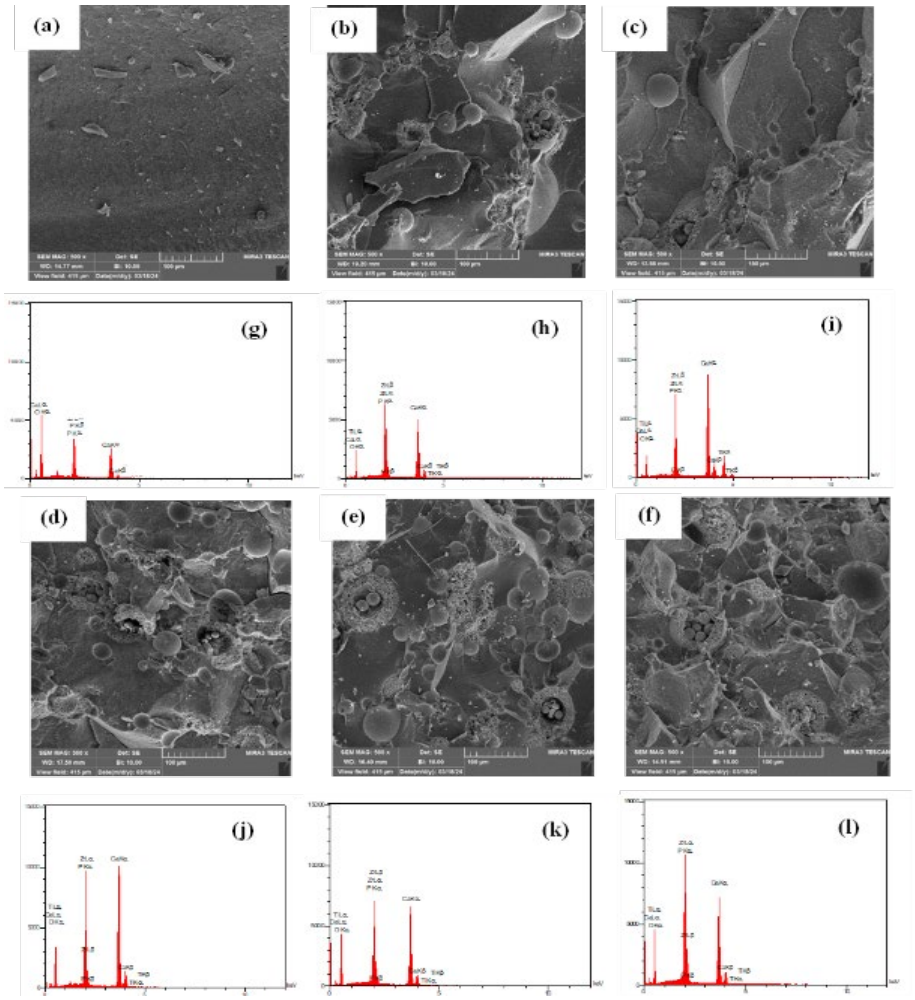

Figure 3. FESEM images (a) 100-0-0, (b) 90-6-4, (c) 81-15-4, (d) 75-21-4, (e) 70-26-4, (f) 65-31-4, and EDX (g) 100-0-0, (h) 90-6-4, (i) 81-15-4, (j) 75-21-4, (k) 70-26-4, and (l) 65-31-4 of sintered HA-YSZ-Ti composite samples fracture surface.

Table 3. EDX analysis results of sintered composite samples.

Sample code	%Weight					Ca/P
	O	P	Ca	Ti	Zr	
100-0-0	63.91	14.51	27.57	0	0	1.15
90-6-4	38	8.57	30.52	0.98	2.19	3.56
81-15-4	37.15	10.07	32.97	0.81	5.11	3.27
75-21-4	44.61	16.71	30.76	0.63	7.29	1.84
70-26-4	45.21	8.51	26.57	0.88	18.83	3.12
65-31-4	41.61	9.40	26.28	0.73	21.97	2.79

Table 4. The first and second gas output values, the amount of displacement occurred during sintering and the maximum temperature of the sintering for different produced samples.

Sample code	First gas exit temperature range		Second gas exit temperature range		The amount of first gas exit	Second gas output amount	Displacement amount	Completion of sinter	The maximum temperature of the sinter [°C]
	Start [°C]	End [°C]	Start [°C]	End [°C]	[X10 Pa]	[X10 Pa]	[mm]		
100-0-0	116	544	544	778	2.7	5.6	10.2	Yes	854
90-6-4	150	604	604	799	3.8	1.6	7.9	Yes	800
81-15-4	142	596	596	847	3.3	2.4	7.8	Yes	861
75-21-4	111	621	621	-	2	1.2	7.9	No	751
70-26-4	95	618	618	-	3.1	2.2	7.1	Yes	854
65-31-4	113	583	583	792	2.6	2.2	7.3	Yes	879

The EDX results of sintered composite samples are presented in Table 3. In stoichiometric hydroxyapatite, the weight percentage and molar ratios of calcium to phosphorus are 2.15 and 1.67, respectively. A deviation can be detected in the weight percentage of calcium to phosphorus in the sintered composite samples from the value of 2.15 due to the deviation from the stoichiometric ratio as a result of the hydroxyapatite formation and the dissolution of calcium in the zirconia network.

3.4 Investigating the sintering behavior of composite samples

3.4.1 Investigating changes in displacement and vacuum pressure during the sintering process

The powder composition of the samples was poured into the mold and placed inside the SPS machine. By increasing the current, the sample was heated up. The values of temperature, displacement, and vacuum were recorded during sintering as shown in Figure 4. During sintering, the absorbed and structural waters were released, causing a gas release. In the continuation, when the sintering of the samples occurred, an increase in temperature caused by sparking led to the decomposition of hydroxyapatite and the formation of tricalcium phosphate at the place of the sparks, causing the second gas release. The first and second gas output values, the amount of displacement occurred during sintering, and the maximum temperature of the sintering of different samples are listed in Table 4.

According to Table 4, the extent of displacement during sintering decreased by reducing the HA content.

The results of the second gas emission of the sintered samples are depicted in Figure 5. Since the release of the second gas was exactly at the same time as the sintering of the samples, it was related to the increase in temperature at the place of the sparks and between the powder particles, and this increase in temperature led to the decomposition of hydroxyapatite and the release of gas in these places.

In SPS, gas release matters because the rapid kinetics of densification can outpace the kinetics of gas escape. This leads to trapped gas pockets that hinder densification by counteracting the applied pressure and degrade microstructure by creating residual porosity, causing abnormal grain growth, and potentially leading to catastrophic defects like cracking [21].

3.4.2 The porosity of sintered composite samples

Porosity percentage of sintered composite samples was calculated by the Archimedes method as presented in Figure 6. By incorporation of YSZ into hydroxyapatite, the porosity percentage decreased, leading to denser samples. The porosity, however, rose with further increase of YSZ content, such that the porosity reached 4.6% and 4.5% in samples 70-26-4 and 65-31-4, respectively.

3.5 Mechanical properties

3.5.1 Three-point flexural strength

Three-point bending test was performed on the sintered composite samples. The three-point flexural strength of the samples was calculated based on the maximum force values obtained from the force-displacement diagrams and Equation (1) as shown in Figure 7.

The flexural strength of sample 100-0-0 was about 30 MPa which rose to 44 MPa by adding YSZ and titanium (90-6-4, the sample with the highest value).

By increasing the content of YSZ, the flexural strength decreased and reached 18 MPa which remained constant in 75-21-4 sample and slightly increased in the samples 70-27-3 and 65-31-4.

The trend can be explained by the competing effects of micro-structural density (porosity) and the formation of various phases in composite. The specimen 90-6-4 exhibits the highest flexural strength. This indicates that this specific composition condition results in the

most favorable microstructure. According to Figure 6, It likely has the lowest porosity percentage. The ratio of components (90-6-4) probably allows for the optimal formation of a strong, interlocking grain structure or a densified binding phase.

Generally, the decomposition temperature of apatite is reduced by adding secondary phases to hydroxyapatite. This was consistent with the results of Salehi *et al.* and Fatemi *et al.* who reported that adding YSZ to hydroxyapatite powder increased the sintering temperature and reduced thermal decomposition of hydroxyapatite [15,16].

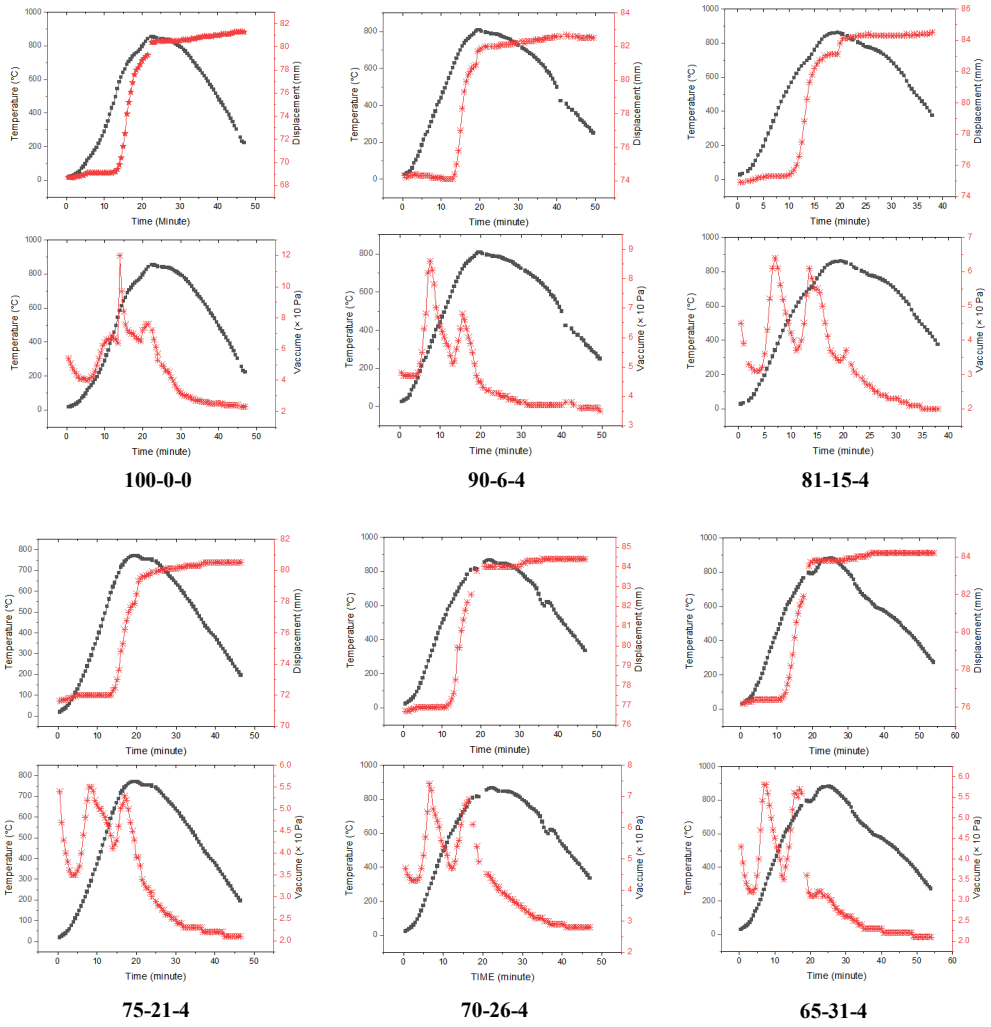

Figure 4. Temperature-displacement and vacuum-temperature graphs in terms of time for sintered composite samples.

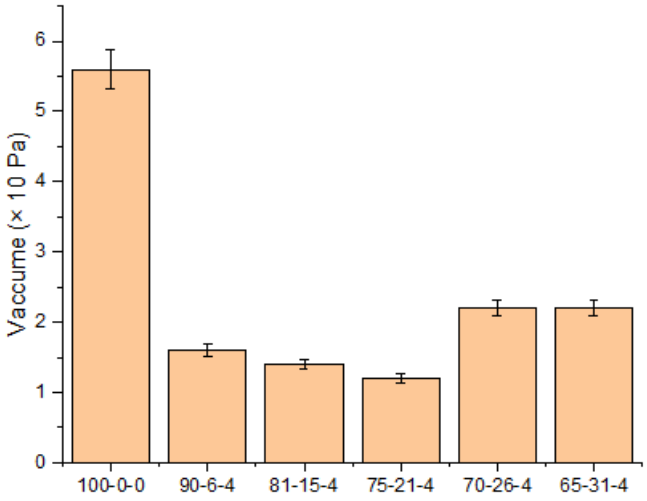

Figure 5. The results of second gas release of sintered samples.

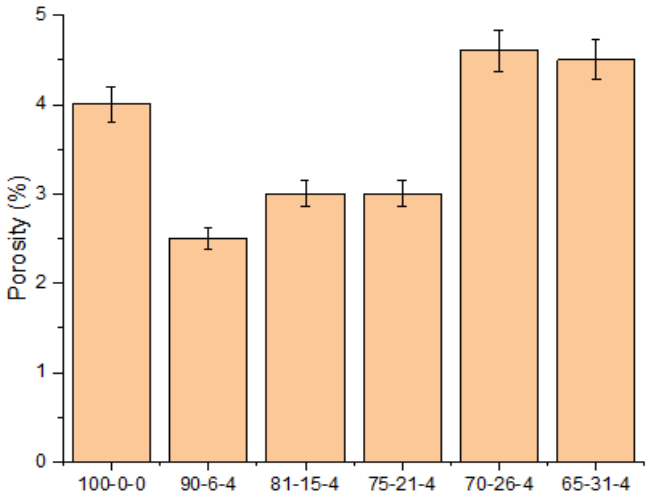

Figure 6 Porosity percentage of sintered composite samples.

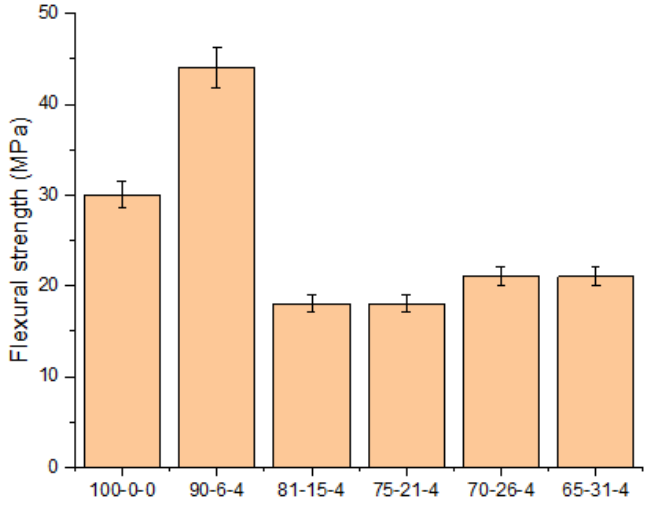

Figure 7. Flexural strength results of sintered composite samples.

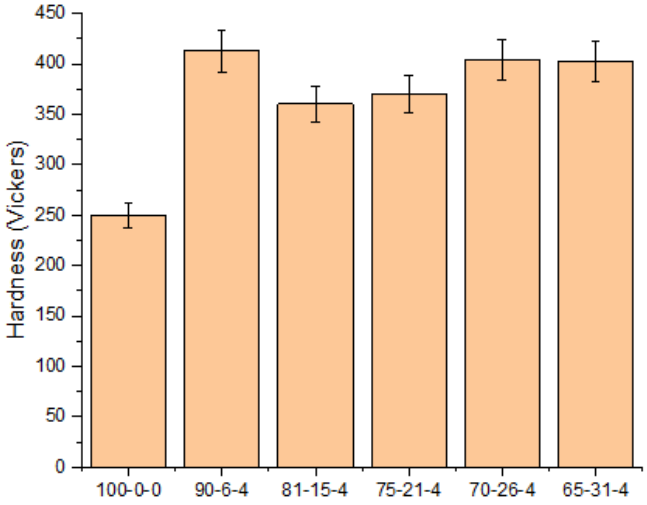

Figure 8. Vickers hardness values of sintered composite samples.

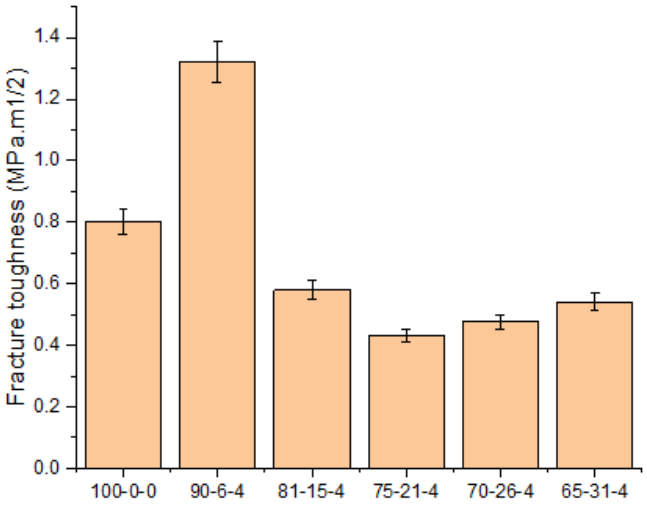

Figure 9. Fracture toughness values of sintered composite samples.

The change in composition from the optimal condition likely introduces more porosity. The significant drop in strength for 81-15-4 and 75-21-4 is classic behavior caused by a deterioration of the microstructure. By adding secondary phases YSZ and Ti to the Hydroxyapatite matrix, the presence of phase TCP resulting from the decomposition of Hydroxyapatite is evident in the X-ray diffraction patterns in Figure 2. With increasing addition of the amount of secondary phases, the intensity of the peaks of phase TCP resulting from the decomposition has increased. The greater the decomposition rate of hydroxyl groups, the greater the release of exhaust gases and, consequently, the increased porosity. In 70-27-3 and 65-31-4 specimens the slight recovery in strength, while not reaching the initial high, suggests that a new, more stable microstructural arrangement is being formed. While porosity remains higher than in the optimal sample, the intrinsic strength of a more favorable pore structure provides a slight recovery in overall flexural strength. The conclusion drawn from this section was that the sintered composite samples containing 10% additive showed the highest flexural strength which is consistent with Mohd nor Rulhadi [22] and Ebrahimi [18].

3.5.2 Hardness

The hardness of the sintered composite samples in terms of Vickers units is shown in Figure 8. The hardness value of sample 100-0-0 was 250 Vickers which reached 413 Vickers (the highest level) in sample 90-6-4. With the further increase of YSZ in samples 81-15-4 and 75-21-4, this value decreased and reached 360 Vickers and 370 Vickers, respectively. In samples 70-26-4 and 65-31-4, this value was about 400 Vickers.

In this part, it was found that the highest hardness of the samples was for a sample containing 90% hydroxyapatite and 10% YSZ and titanium additives, and this was consistent with the results obtained in the research of Mohd nor Rulhadi [22]. Also, thermal decomposition and formation of TCP led to a decrease in hardness in samples 81-15-4 and 75-21-4, and in samples 70-26-4 and 65-31-4, with the dissolution of calcium oxide in the YSZ structure, the hardness of It increased.

3.5.3 Fracture toughness

The fracture toughness of the samples are shown in Figure 9. The fracture toughness of sample 100-0-0 was 0.8 MPa.m0.5 which grew to 1.32 MPa.m1/2 in the sample 90-6-4 by reducing hydroxyapatite and increasing YSZ contents. With further increase of YSZ content, this value decreased so that the sample 75-21-4 showed the toughness value of 0.43 MPa.m0.5. With further increase of YSZ, the toughness slightly increased and reached 0.54 MPa.m1/2 in sample 65-31-4.

The results of the sintered samples showed the occurrence of thermal decomposition in all the samples. Thermal decomposition and the formation of TCP phase increased by declining HA and the increasing YSZ levels, declining the flexural strength, hardness and fracture toughness. These variations were accompanied by a reduction in mechanical properties. On the other hand, the presence of YSZ and titanium increased the mechanical properties up to 10%, The increase in mechanical properties exceeds the decrements in mechanical properties due to the formation of TCP phase. However, with an increase in thermal decomposition, the formation of calcium oxide rose which could enter the YSZ structure, further promoting the stability. It lowers the thermal decomposition and the formation of TCP phase, resulting in an improvement in the mechanical properties.

4. Conclusions

During sintering, as the composite samples were heated, the adsorbed and structural waters are released, leading to the release of gas. In the continuation, the sintering process and increased temperature caused by sparking promote HA decomposition and the formation of tricalcium phosphate at the place of the sparks, causing the second gas release. With further increase in sintering temperature, the third gas emission also occurred in samples 81-15-4 and 65-31-4, which meant further decomposition of hydroxyapatite and formation of TCP phase, which led to a decrease in mechanical properties. On the other hand, increasing the amount of YSZ led to the entry of calcium oxide resulting from the decomposition of hydroxyapatite into the YSZ structure and complete saturation, which led to an improvement in mechanical properties, which was evident in samples 70-26-4 and 65-31-4. It was found that to achieve better mechanical properties (flexural strength, hardness, and toughness), the HA content should be 90% which the levels of YSZ and titanium additives should sum up to 10% wt.

Data Availability

The data that support the findings of this study are available on request from the corresponding author. Declarations

Conflict of Interest The authors declare no competing interests.

Funding

The authors declare that no funds, grants, or other support were received during the preparation of this manuscript.

Author Contributions

Seyed Mohsen Fatemi: Formal analysis, Investigation, Methodology, Writing - original draft; Iman Mobasherpour: Validation, Writing - review & editing; Project administration; Liela Nikzad: Conceptualization, Supervision; Mansour Razavi: Validation, Supervision. All authors read and approved the final manuscript.

Acknowledgements

The authors of the manuscript are grateful to the experts of the Central Laboratory of Materials and Energy Research Center.

References

[1] T. Biswal, S.K. BadJena, and D. Pradhan, "Sustainable biomaterials and their applications: A short review," *Materials Today: Proceedings*, vol. 30, pp. 274–282, 2020.

[2] H. Kolemek, I. Bulduk, Y. Ergun, S. E. Korcan, R. Liman, M. Konuk, and F. K. Coban, "Studies on toxicity of noscapine loaded hydroxyapatite nanoparticles," *Sigma Journal of Engineering and Natural Sciences*, vol. 41, no. 824, pp. 824–836, 2023.

[3] I. Mobasherpour, M. Soulati Heshajin, A. Kazemzadeh, M. Zakeri, "Synthesis of nanocrystalline hydroxyapatite by using precipitation method," *Journal of Alloys and Compounds*, vol. 430, no. 1–2, pp. 330–333, 2007.

[4] S. Moharana, Y. Otsuka, and R. Gnanamoorthy, "Enhancing the fretting damage resistance of suspension plasma sprayed hydroxyapatite coating with Titania addition," *Surface and Coatings Technology*, vol. 476, p. 130236, 2024.

[5] Y. Seo, T. Goto, S. Cho, and T. Sekino, "Densification of transparent hydroxyapatite ceramics via cold sintering process combined with biomineralization," *Journal of the European Ceramic Society*, vol. 44, no. 6, pp. 4285–4293, 2024.

[6] F. Saji, I. Mobasherpour, L. Nikzad, M. Razavi, M.O. Shabani, "Microstructural analysis and electrochemical behavior of functional gradient coating hydroxyapatite/tricalcium phosphate on Ti-6Al-4 V by plasma spraying method," *Brazilian Journal of Physics*, vol. 53, no. 6, Art. no. 151, 2023.

[7] C. R. D. Ferreira, A. A. G. Santiago, R. C. Vasconcelos, D. F. F. Paiva, F. Q. Pirih, A. A. Araújo, F. V. Motta, and M. R. D. Bomio, "Study of microstructural, mechanical, and biomedical properties of zirconia/hydroxyapatite ceramic composites," *Ceramics International*, vol. 48, no. 9, pp. 12376–12386, 2022.

[8] F. A. Anene, C. A. N. Jaafar, A. H. M. Ariff, I. Zainol, S. M. Tahir, B. A. Razak, M. S. Salit, J. A. Amaechi. "Biomechanical properties and corrosion resistance of plasma-sprayed fish scale hydroxyapatite (FsHA) and FsHA-doped yttria-stabilized zirconia coatings on Ti–6Al–4V alloy for biomedical applications," *Coatings*, vol. 13, no. 1, 2023.

[9] N. P. Msweli, S. O. Akinwamide, P. A. Olubambi, and B. A. Obadele, "Microstructure and biocorrosion studies of spark plasma sintered yttria stabilized zirconia reinforced Ti_6Al_7Nb alloy in Hanks' solution," *Materials Chemistry and Physics*, vol. 293, p. 126940, 2023.

[10] P. Diana Julaidy, N. Ari Dwi, A. Ika Dewi, and Y. Yusril, "Mechanical characteristics and bioactivity of nanocomposite hydroxyapatite/collagen coated titanium for bone tissue engineering," *Bioengineering*, vol. 9, no. 12, 2022.

[11] M. A. N. Zainurin, I. Zainol1, Ch. A. Jaafar, and M. Mudhafar, "The effect of yittria-stabilized zirconia (YSZ) addition on the synthesis of beta-tricalcium phosphate from biogenic hydroxyapatite," *Malaysian Journal of Microscopy*, vol. 19, no. 1, pp. 66–75, 2023.

[12] B. Ratzker, and M. Sokol, "Exploring the capabilities of high-pressure spark plasma sintering (HPSPS): A review of materials processing and properties," *Materials and Design*, vol. 233, p. 112238, 2023.

[13] Y. Le. Godec, and S. Le. Floch, "Recent developments of high-pressure spark plasma sintering: An overview of current applications, challenges and future directions," *Materials*, vol. 16, no. 3, p. 997, 2023.

[14] E. L. Medina, J. J. Vaca-Gonzalez, W. Aperador, S. Ramtani, C. F. Daudre, and D. G. Alvarado, "Review of advanced coatings for metallic implants: A study/proposal on yttria-stabilized zirconia and silver-doped hydroxyapatite," *JOM*, vol. 77, no. 1, pp. 5345–5361, 2025.

[15] S. M. Fatemi, I. Mobasherpour, L. Nikzad, M. Razavi, L. Karamzadeh, "Effect of chemical composition on fabrication

of HAp-YSZ-Ti composites by spark plasma sintering method," *Synthesis and Sintering*, vol. 4, no. 3, pp. 160–166, 2024.

[16] S. Salehi, M. H. Fathi, and K. Raeissi, "Fabrication and characterization of nanostructured hydroxyapatite (HA)/yttria stabilized zirconia (YSZ) composite coatings with various contents of yttria," *Journal of Advanced Materials in Engineering (Esteghlal)*, vol. 29, no. 1, pp. 31–43, 2010.

[17] P. Chantikul, G. R. Anstis, B. R. Lawn, and D. B. Marshall, "A critical evaluation of indentation techniques for measuring fracture toughness: I, direct crack measurements," *Journal of the American Ceramic Society*, vol. 64, no. 9, pp. 533–538, 1981.

[18] M. Ebrahimi, I. Mobasherpour, H. Barzegar Bafrooei, F. S. Bidabadi, M. Mansoorianfar, Y. Orooji, A. Khataee, C. Mei, E. Salahi, T. Ebadzadeh, "Taguchi design for optimization of structural and mechanical properties of hydroxyapatite-alumina-titanium nanocomposite," *Ceramics International*, vol. 45, no. 8, pp. 10097–10105, 2019.

[19] R. B, Heimann, T. A, Vu, "Effect of CaO on thermal decomposition during sintering of composite hydroxyapatite-zirconia mixtures for monolithic bioceramic implants," *Journal of Materials Science Letters*, vol. 16, pp. 437–439, 1997.

[20] Z. Evis, C. Ergun, and R. H. Doremus, "Hydroxylapatite-zirconia composites: Thermal stability of phases and sinterability as related to the CaO-ZrO_2 phase diagram," *Journal of Materials Science*, vol. 40, pp. 1127–1134, 2005.

[21] R. M. German, "Sintering Theory and Practice" Publisher: John Wiley & Sons, 1996.

[22] N. M. N. Rulhadi, N. A. Rahim, A. M. Sharif, and I. Zainol, "Effect of yttria stabilized zirconia addition in natural hydroxyapatite composites for dental restoration," *Solid State Science and Technology*, vol. 26, no. 2, 2018.